Environmental Science Processes & Impacts

PAPER

View Article Online
View Journal | View Issue

Cite this: *Environ. Sci.: Processes Impacts*, 2024, **26**, 1205

Effects of burning and photochemical degradation of Macondo surrogate oil on its composition and toxicity†

Pamela P. Benz, *[a] Phoebe Zito, [b] Ed Osborn,[b] Aleksandar I. Goranov, [c] Patrick G. Hatcher,[c] Matthew D. Seivert [d] and Wade H. Jeffrey [e]

Received 17th January 2024
Accepted 2nd June 2024

DOI: 10.1039/d4em00023d

rsc.li/espi

Petroleum products in the environment can produce significant toxicity through photochemically driven processes. Burning surface oil and photochemical degradation were two mechanisms for oil removal after the Deepwater Horizon (DWH) oil spill in the Gulf of Mexico. After burning, residual oil remains in the environment and may undergo further weathering, a poorly understood fate. Although photochemistry was a major degradation pathway of the DWH oil, its effect on burned oil residue in the environment is under studied. Here, we ignited Macondo surrogate crude oil and allowed it to burn to exhaustion. Water-accommodated fractions (WAFs) of the burn residue were created in full sunlight to determine the effects of photochemical weathering on the burned oil residue. Our findings show that increased dissolved organic carbon concentrations (DOC) for the light unburned and light burned after sunlight exposure positively correlated to decreased microbial growth and production inhibition (*i.e.* more toxic) when compared to the dark controls. Optical and molecular analytical techniques were used to identify the classes of compounds contributing to the toxicity in the dark and light burned and dark and light unburned WAFs. After light exposure, the optical composition between the light unburned and light burned differed significantly ($p < 0.05$), revealing key fluorescence signatures commonly identified as crude oil degradation products. Fourier transform ion cyclotron resonance mass spectrometry (FT-ICR MS) analysis showed more condensed aromatic, reduced oxygenated compounds present in the light burned than in the light unburned. FT-ICR MS also showed an increase in the percent relative abundance of carboxyl-rich alicyclic molecules (CRAM) like compounds in the light burned compared to light unburned. The increase in CRAM suggests that the composition of the light burned is more photorefractory, *i.e.*, reduced, explaining the residual toxicity observed in microbial activity. Overall, these data indicate burning removes some but not all toxic compounds, leaving behind compounds which retain considerable toxicity. This study shows that burn oil residues are photolabile breaking down further into complex reduced compounds.

Environmental significance

Burning surface oil and sunlight oxidation were two key mechanisms for oil removal after the Deepwater Horizon oil spill in the Gulf of Mexico. Burning selectively removed some toxicity, but residual toxicity remained in the water column, especially once burn residues were in sunlight. The changes in the composition of the burn residue observed after FS treatment is evident that photo dissolution is a major pathway to consider for when using *in situ* burning as a remediation tool. These results add important new information regarding using *in situ* burning as a remediation tool for spilled surface oil in aquatic systems. Burned oil may negatively impact ecosystem health when petroleum is exposed to sunlight.

[a]*Department of Chemistry, University of West Florida, 11000 University Parkway, Pensacola, FL 32514, USA. E-mail: pamelabenz@uwf.edu*

[b]*Department of Chemistry, Chemical Analysis & Mass Spectrometry Facility, University of New Orleans, New Orleans, LA 70148, USA*

[c]*Department of Chemistry and Biochemistry, Old Dominion University, Norfolk, VA 23529, USA*

[d]*Department of Chemistry, University of Georgia, 140 Cedar Street, Athens, GA 30602, USA*

[e]*Center for Environmental Diagnostics and Bioremediation, University of West Florida, 11000 University Parkway, Pensacola, FL 32514, USA*

† Electronic supplementary information (ESI) available. See DOI: https://doi.org/10.1039/d4em00023d

1 Introduction

Since the 1960s, *in situ* burning has been used to remove spilled oil on surface water to help mitigate the negative environmental impacts of an oil spill. The technique involves igniting the oil and converting it to combustion products, which prevents further transport of spilled oil to coastal regions. In 2010, the Deepwater Horizon oil spill released over 4.9 million barrels of Macondo well oil in the Gulf of Mexico.[1] Most spilled petroleum was subjected to mechanical recovery, chemical dispersion, and

burning.[2] An estimated 220 000 to 310 000 barrels of Macondo crude oil, or about 5% of the released oil, was burned between April 28 and July 19, 2010.[3,4] The effectiveness and environmental impacts of *in situ* burning depend on many factors, including the geographic location of the spill, oil type, and weather conditions.[5] Therefore, it is not universally applicable to every spill, and its environmental impacts are not fully understood.

Environmental risks associated with burning oil remain controversial. An advantage of *in situ* burning is that it prevents surface petroleum from reaching shorelines by reducing the volume of surface petroleum (including lower molecular weight and volatile compounds). The disadvantages are that it produces combustion by-products like black carbon and smoke.[6,7] Smoke released into the atmosphere has been shown to produce "black carbon" particulates (PM2.5 particles), which have significant human health impacts. The formation of combustion by-products, including pyrogenic polycyclic aromatic hydrocarbons (PAHs) and sulfur-containing thiophenes, known carcinogens, have been reported.[8,9]

Previous research has shown *in situ* burning of petroleum enriches pyrogenic PAHs depleting terpenes, steranes, and triaromatic steroids.[4] Jaggi *et al.* reported a loss of low molecular weight alkanes, enrichment of condensed aromatics (dibenzothiophenes and phenanthrenes), and increased oxygenation with resulting greater aqueous solubility in burned Macondo oil (MC252).[10] Chemical transformations caused by burning may have implications that negatively impact long-term ecosystem health. Despite these studies, little attention has focused on the photo-enhanced dissolution of burned and unburned residual oil after sunlight exposure and its subsequent impact on microorganism growth. Due to its high complexity, advanced analytical instrumentation is required to identify burn products in the oil and water phases.

Techniques such as Fourier transform-ion cyclotron resonance mass spectrometry (FT-ICR MS) and tandem two-dimensional gas chromatography have allowed researchers to characterize petroleum and petroleum-derived complex mixtures.[11,12] Huba and Gardinali (2016) examined weathered petroleum using FT-ICR-MS with various ionization methods, including electrospray ionization (ESI) and atmospheric pressure photoionization (APPI).[13] It is well-known that photo-oxidation increases oxygenated heteroatom species in oil and water fractions (also known as water-accommodated fractions or WAFs).[13–15] Increasing oxygenation with weathering formed ketonic and quinonic species,[13] oxygenated polyaromatic hydrocarbons (oxyPAHs),[16,17] naphthenic acid and carboxylic acids,[18–23] carbonyl compounds[24,25] and others upon photo-irradiation. Additionally, increased toxicity was observed for irradiated WAFs.[15,26]

Although burning is a common method of oil remediation, there are a limited number of studies characterizing transformations during combustion and even fewer studies examining environmental effects, such as aquatic toxicity. The environmental impact of burned by-products and the effect of sunlight on the fate of burned oil residues in aquatic systems require further investigation. The purpose of this study is to (1) assess the toxicity of photodegraded unburned and burned WAF generated from residues, (2) measure the dissolved organic carbon concentration in each WAF fraction, (3) identify compositional differences in the burned and unburned oil residues using FT-ICR-MS, (3) perform chemical analyses on burned and unburned WAF using optical techniques and (4) identify compositional classes potentially inhibiting bacterial growth production. The knowledge gained from this study will evaluate the impact of *in situ* burning as a remediation tool for spilled oil in aquatic systems and provide data which can be included in photochemical models for future spills.

2 Experimental

2.1 Materials

3H-Leucine (54 Ci mmol^{-1}) and 14C-bicarbonate were obtained from PerkinElmer. ECOLUME liquid scintillation cocktail was purchased from MP Biomedicals. Surrogate crude oil was obtained from AECOM, Ft. Collins, CO (A0063S).

2.2 Methods

2.2.1 Burning procedure. Oil was burned in the lab by placing 8 replicate 25 mL oil samples in pre-cleaned glass baking pans resulting in a thin layer (~1 mm thick) of oil that just covered the bottom of the pan. The remaining burned oil residues were then combined and used to create WAFs as described below.

2.2.2 Creation of water accommodated fractions (WAF). WAFs were created using aged seawater originally collected from offshore Gulf of Mexico waters and allowed to age for 3 years in the lab to promote degradation of all labile carbon (DOC = 2.6 mg C per L). Once aged, the seawater was gently filtered through a 0.2 μm pore-sized polycarbonate filter and then Pasteurized for a minimum of 2 h at 70 °C in 1 L Teflon bottles. Parent surrogate oil and burned oil were added to a final concentration of 1% by volume consistent with ranges published in the CROSERF protocols.[27] WAFs were generated during summer months in Pensacola, FL (30.55° N) in recirculating water baths on the roof of building 58 at the University of West Florida at a constant temperature of 20 °C. The Teflon bottles had light transmittance: 86% at 295 nm; 90% at 350 nm; and 95% at 465 nm. Sample treatments included full solar spectrum (FS) exposure and in the dark by wrapping in aluminum foil. Incident solar irradiance was monitored during the production of WAFs using a Biospherical Instruments GUV511 solar radiometer mounted next to the water baths. After five days of exposure, WAFs were collected from the bottom of each bottle.

2.2.3 Bacterial production and phytoplankton primary production. Seawater used for the toxicity assays was collected from the end of the pier at Pensacola Beach, FL (30° 19.640′ N, 87° 08.514′ W) and transported back to our lab at *in situ* temperature in the dark. Bacterial growth was determined by incorporating 3H-leucine as an indicator of protein synthesis and a proxy for bacterial growth rates. Using the method described in Vaughan *et al.* (2016), samples were prepared in

triplicate and amended with 3H-leucine (54 Ci $mmol^{-1}$ PerkinElmer, Bridgeport, CT) to a final concentration of 10 nM.[15] Using Smith and Azam's microcentrifuge method, incorporation into trichloroacetic acid precipitable fractions was determined.[28] Incorporated 3H-leucine was quantified through liquid scintillation counting using a Packard Tri-Carb 2900. Percent inhibition caused by specific WAFs was compared to the unamended controls.

Phytoplankton growth efficiency was estimated from traditional Photosynthesis *vs.* Irradiance (P *vs.* I) curves using the fixation of 14C-bicarbonate (1 μCi mL^{-1}) under increasing light exposure. Photosynthetic efficiency was determined as the slope of the fixation data during the initial linear part of the curve.[29] WAFs were added to seawater at 10% volume for this part of the study.

2.3 Analysis

2.3.1 Quantification of solar radiation dosage. Cumulative solar radiation dosage for WAF exposure was monitored using a Biospherical Instruments (San Diego, CA) model GUV511 solar radiometer monitoring 305 nm = 0.51 J cm^{-2} nm^{-1}, 320 nm = 3.00 J cm^{-2} nm^{-1}, 340 nm = 8.00 J cm^{-2} nm^{-1}, 380 nm = 4.00 J cm^{-2} nm^{-1} and Photosynthetically Active Radiation (PAR; 400–700 nm) = 20 788 mmol cm^{-2} over five days.

2.3.2 Dissolved organic carbon analyses. Dissolved organic carbon (DOC) concentrations in WAF samples were obtained by filtering using 0.27 μm filters (Advantec GF–75) and acidified to pH 2 with concentrated ultra-high purity HCl (BDH ARISTAR® PLUS). DOC was measured on a Shimadzu TOC-VCSH Total Organic Carbon Analyzer with an ASI-V autosampler. The instrument employs a combination of high-temperature combustion/non-dispersive infrared detector (NDIR) techniques. The acidified samples are sparged with ultra-zero-grade purified air for 5.5 minutes to remove any purgeable organic carbon. Samples were injected into a combustion tube containing a platinum catalyst and heated, oxidizing all carbon-containing compounds in the sample to CO_2 gas. The CO_2 generated by oxidation is detected *via* the absorbance of infrared radiation in the NDIR. DOC was quantified using five-point calibration curves of potassium hydrogen phthalate (99.5%; Sigma Aldrich), was dried at 110 °C for 4 hours before use. DOC data are reported as mg of carbon per L (mg C per L).

Five-point calibration curves were used with a final 20 mg C per L concentration. A 20 mg C per L stock was prepared from the reference standard, and the instrument was programmed to dilute to intermediate calibration points automatically using pH 2 acidified nanopure water. A 5 mg C per L control was prepared and injected after each calibration curve and every 10 sample injections to maintain system suitability throughout the analyses. Sample sequence was created with bracketed calibration curves at the beginning and end of each run. Acidified nanopure washes were performed after each injection to prevent carryover. Sample 1% dark burn was a significant outlier ($\rho < 0.05$). This may have been due to contamination from the broken sample vials during shipment. Outliers were calculated using the GraphPad QuickCalcs Web site: **https://www.graphpad.com/quickcalcs/ConfInterval1.cfm** (accessed November 2015). Five sample replicates for the dark burned and unburned and light unburned were broken during shipment for water chemistry analysis at UNO. Therefore, two additional dark WAFs were prepared from the burned and unburned oil and all chemical analyses were repeated.

2.3.3 Fluorescence spectroscopy. Sixteen WAF samples were adjusted to pH 8 for fluorescence spectroscopy measurements on a Horiba Aqualog fluorimeter (Horiba Scientific, Kyoto, Japan).[30] Excitation–emission matrix (EEM) measurements were conducted at constant room temperature using a 10 mm quartz cuvette. Weekly checks are performed to test instrument stability before analysis using a sealed water cell (Starna Raman Ultra-Pure Water, Certified Reference material # 1264 RM-H_2O) to determine the Raman peak of water. Nanopure water blanks were checked daily before sample collection. The excitation and emission wavelengths were scanned from 240 to 800 nm at 5 and 2 nm increments, respectively. Nanopure water was used for dilution correction to a 254 nm < 0.1 to reduce inner-filter effects, as reported in Zito *et al.* 2019.[31] Parallel Factor (PARAFAC) analysis was conducted to determine the underlying spectral properties of the EEMs (Fig. S4†) using the drEEM toolbox 0.6.5.[32] A nanopure water blank was subtracted, and the spectral intensities were corrected for Rayleigh and Raman scattering during PARAFAC analysis.[33] PARAFAC components were uploaded onto the OpenFluor database[34] and were compared to previously reported DOM datasets from other studies using a minimum similarity threshold of 95%. HIX values were calculated from the emission intensity in ranges of 435–480 nm and 300–345 nm with an excitation of 254 nm.[35]

2.3.4 FT-ICR-MS analysis. WAF samples were uniformly diluted to DOC of 50 mg C per L and solid-phase extracted using 50 mg Agilent PPL cartridges into 100% MeOH following Dittmar *et al.* 2008.[36] Uniform DOC and consistent sample preparation are critical for ensuring maximum sample comparability, especially prior to multivariate statistical analysis. Methanolic eluents were shipped to Old Dominion University for Fourier transform ion cyclotron resonance mass spectrometry (FT-ICR MS) analysis on a Bruker Daltonics 10 Tesla Apex Qe system at the College of Sciences Major Instrumentation Cluster (COSMIC) facility. Samples were directly injected into an Apollo II ESI source operated in negative mode. The instrument was tuned with a polyethylene glycol standard,[37] and the Suwannee River FA (SRFA) standard from the International Humic Substances Society was used to validate the tune and ensure data reproducibility following the recommendations by Hawkes *et al.* (2020).[38] A representative methanolic eluent diluted ×2 was compared to a water-spiked sample (1 : 1 MeOH : H_2O) to determine the most optimal analysis conditions. As 1 : 1 MeOH : H_2O conditions produced more stable ionization currents, all samples were prepared this way and analysed with the same tuning parameters to prevent instrumental variability from influencing the spectral comparability. All samples yielded spectra characteristic of natural organic matter indicative of clean sample preparation and lack of significant background contaminants. Furthermore, a pure methanol blank was run for

30 s between each two samples to ensure no carryover. Notably, an aged seawater black was not analysed indicating that some formulae belonging to background DOM will be present in the WAF molecular catalogues and should be thus considered during the data analysis and interpretations.

2.3.5 Mass calibration and data analysis. Following the acquisition, spectra were internally calibrated using naturally present fatty acids, dicarboxylic acids, and compounds belonging to CH_2-homologous series.[39] Peaks with signal-to-noise ratio ≥3 were used for formula assignment. Peaks of two procedural blanks, peaks of inorganic origin ("salt" peaks), and isotopologue (^{13}C, ^{34}S) peaks were removed to obtain a list of peaks corresponding to molecular DOM species as described by Goranov *et al.* (2023).[40] Peak lists were aligned following to average out *m*/*z* values and obtain lower assignment errors.[41] Molecular formulae were assigned using a previously published MATLAB script.[42] The assignment was limited to $^{12}C_{5-\infty}$, $^{1}H_{5-100}$, $^{16}O_{1-50}$, $^{14}N_{0-4}$, $^{32}S_{0-2}$, with a maximum assignment error of 1 ppm. Formulae that did not adhere to previously established molecular rules for natural organic matter[43–45] were eliminated. Peaks with any residual ambiguous assignments (multiple possible molecular formulae per mass peak) were further refined using inclusion within homologous series (CH_2, H_2, COO, CH_2O, C_2H_4O, O, H_2O, NH_3).[43,45] Any further ambiguous assignments were refined based on assignment error, and the molecular formula with a lower assignment error was selected. There was only one molecular formula per mass peak in the final list of molecular formulae for each sample. Obtained formula catalogs were further refined to (1) remove all CHONS, (2) remove O/C < 0.08, (3) remove O/C > 0.8, and remove (4) H/C < 0.5 as common formula catalog curation procedures for petroleum-derived samples.[30] For all samples at least 80% of the assignable WAF peaks were annotated with a molecular formula, and the annotated peaks accounted for at least 85% of the spectral intensity. Formula assignment and refinements were done using the Toolbox for Environmental Research (TEnvR) in MATLAB 2022a, as described by Goranov *et al.* (2023).[39,40] Select formulae from the catalogs were assessed manually to confirm their correct assignment (*e.g.*, formulae from suspiciously looking clusters of low O/C and H/C ratios). Molecular formulae were classified into categories based on stoichiometry into condensed aromatic (CA) modified aromaticity index (AImod ≥ 0.67), aromatic (0.67 > AImod ≥ 0.5), unsaturated low oxygen (ULO) (AImod < 0.5, H/C < 1.5, O/C < 0.5), unsaturated high oxygen (UHO) (AImod < 0.5, H/C < 1.5, O/C ≥ 0.5), aliphatic (H/C ≥ 1.5) as previously reported.[16]

3 Results and discussion

3.1 Water accommodated fraction inhibits bacterial production after sunlight exposure

The effects of WAFs on microbial production (bacterioplankton and phytoplankton) are illustrated in Fig. 1. No notable difference (ρ > 0.05) was observed for WAF incubated in the dark unburned and dark burned samples. Further, bacterioplankton (Fig. 1, top) and phytoplankton (Fig. 1, bottom) toxicity assays showed similar trends for each treatment. No significant effects

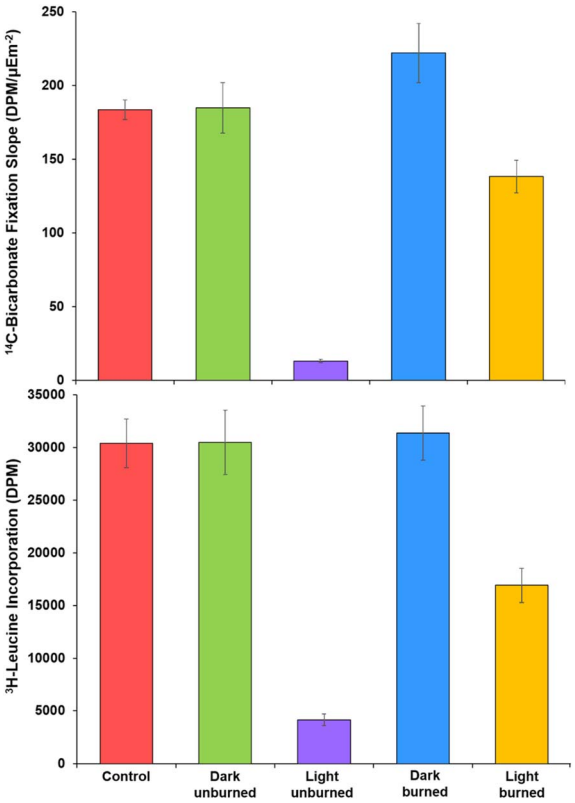

Fig. 1 Comparison of growth responses from phytoplankton primary production (top) and percent inhibition of bacterial production (bottom) from dark unburned (green), light unburned (purple), dark burned (blue), and light burned (gold).

were observed on microbial production rates for each dark treatment compared to unamended controls (ρ > 0.05). However, light unburned and light burned incubated in the full sun (FS) over five days significantly inhibited (ρ < 0.001) microbial production when compared to both dark treatments and control. The effects of burning on microbial production (both bacterioplankton and phytoplankton) from the dark burned are not statistically different compared to the dark unburned and control (ρ > 0.05). These data imply burning removes some, but not all, compounds contributing to toxicity after light exposure.

3.2 Changes in dissolved organic carbon concentrations and optical composition of WAFs

Fig. 2 illustrates that light exposure caused increased dissolved organic carbon (DOC) concentrations for light unburned (purple) and light burned (gold) which corroborates with previous studies investigating the photodissolution of DOC from hydrocarbon sources.[14,16,46–48] Light unburned (purple) samples increased from 5.1 ± 0.05 mg C per L to 56.5 ± 3.4 mg C per L and were statistically different from the dark unburned (green, ρ = 0.001). Although DOC concentrations increased for light burned from 3.5 ± 0.2 mg C per L to 29.1 ± 10.6 mg C per L (gold), they were not statistically different from the dark burned (ρ > 0.05). These data corroborate with both bacterioplankton

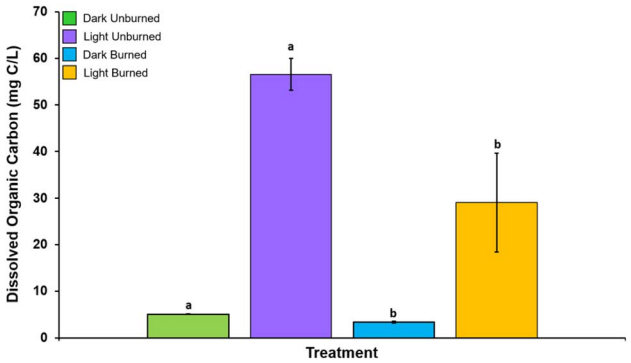

Fig. 2 Dissolved organic carbon concentrations as a function of treatment for dark unburned (green), light unburned (purple), dark burned (blue), and light burned (gold) water accommodated fractions. The letters 'a' and 'b' represent a significant difference between the measurements ($\rho = 2.0 \times 10^{-3}$ and $\rho = 0.05$, respectively).

and phytoplankton assays that some inhibition in microbial production was observed for the light burned but not as significantly as the light unburned which had the greatest growth inhibition. Increasing DOC (ESI Fig. S1†) concentration is strongly correlated ($r > 0.995$) with increasing microbial production inhibition. This relationship suggests that photoproducts produced in the light burned and light unburned fractions may negatively impact microbial production, enhancing biological toxicity similar to previous studies.[26]

Fluorescence spectroscopy determined changes in fluorophoric DOM (fDOM) constituents in unburned and burned samples before and after light exposure. Changes in aromaticity and oxygen content of fDOM were assessed using the humification index (HIX). HIX values for dark unburned were 0.40 ± 0.01 and increased to 0.56 ± 0.0 after sunlight exposure. HIX values for dark burned were 0.48 ± 0.04, increasing to 0.61 ± 0.1 after light exposure. Similar to other studies reporting HIX values for water-soluble petroleum products, increases observed after light exposure indicate relative increases in water-soluble, oxidized, or more "humified" compounds[49,50] which are attributed to compounds with increased aromaticity and oxygen content.[16,35,51,52]

Parallel factor (PARAFAC) analysis revealed four underlying constituents in fDOM (Fig. S2†). The percent relative contribution of each component (C1–C4) is presented in Fig. S3.† The key findings observed from these data were (1) a significant increase in C1 and the appearance of C2 for the light unburned, (3) a significant increase in C2 for the light burned, (4) a significant decrease in C3 for the light burned compared to light unburned, and (5) a substantial decrease in C4 in light unburned after sunlight exposure.

Overall, the PARAFAC components from the dark and light unburned and dark and light burned matched with 166 other studies reporting similar signatures (C1 (23%), C2 (2%), C3 (54%), and C4 (17%)) within Tucker's congruence coefficient (TCC) greater than 95%.

Of these matches, 6 were from petroleum-derived samples matching with C1 (83%), C2 (50%), C3 (50%) and C4 (0.17%) therefore, only these models will be discussed here. The excitation and emission maximum of each component in the PARAFAC model dictates its classification compared to other studies (Fig. S2† in red). Although C1 and C2 fell within the excitation/emission maxima range for components O2 and O3 reported by, (Zhou *et al.*)[53], no OpenFluor matches were observed above 95% TCC. C2 matched with C3 from Zito *et al.* (2019),[31] C1 from Zito *et al.* (2023),[50] C2 from Harsha *et al.* (2023),[16] and C3 from Podgorski *et al.* (2024) which was identified as a new "structural motif" not typically found in non-petroleum-derived.[55]

3.3 DOM samples

Fig. S3† compares treatment to each PARAFAC component illustrating that the main driver for changes to % relative contribution observed in C1 is burning combined with sunlight exposure. These trends are similar to previous studies using PARAFAC in that CDOM/fDOM signatures in C1 are oil-derived photoproducts.[55,56] In agreement with previous studies, C2 was more abundant in the light unburned WAF than the dark unburned WAF. As a result of the significant increase in C2 in light burn, sunlight seems to be the major driver of C2. The presence of C2 fDOM signatures in the dark burned may be due to the presence of more oxidized compounds formed after burning which increase after light exposure. Burning had no significant effect on changes to C3 with and without light. However, a significant decrease was observed for C3 the light unburned WAF.

Overall, these data provide information on the bulk fDOM signatures produced from petroleum sources and how they change after burning and light exposure. The appearance of C2 in the light unburned suggests the formation of oil degradation products, as reported by Zhou *et al.* 2017.[53] Similarly, C1 is also identified as an oil photodegradation component.[53] Statistical differences ($\rho = 0.001$) in % relative contribution for C1 were observed between the light unburned and light burned (Fig. S3† green). The combination of burning and photochemical degradation contributes to a substantial change in fluorophoric composition, producing less carbon in the light burned treatment after sunlight exposure. These findings suggest burning oil decreases the negative impact on microbial growth in water-accommodated fractions of oil. Statistical analyses between each dark and light burned and unburned WAF, are alphabetically illustrated in Fig. S3.† Duplication of each letter within different treatments indicates significant ($\rho < 0.05$) changes in optical composition between each treatment. For example, percent relative contribution of C4 for both dark unburned and burned WAF significantly decreased after sunlight exposure ($\rho < 0.05$) along with a concurrent increase in C3 for light unburned and light burned confirming the production of oil degradation photoproducts.

3.4 Water accommodated fraction (WAF) characterization by FT-ICR-MS

Molecular level characterization of WAF by FT-ICR MS revealed compositional differences between the light unburned and

burned WAF. Molecular catalogs were compared using a presence-absence approach,[57] which identifies the unique formulae in each WAF. Van Krevelen diagrams, which are H/C *versus* O/C plots,[58] are shown on Fig. 3 whereas H/C *versus* molecular weight plots are shown on Fig. S5.† Any commonly shared formulae (including those belonging to background seawater DOM) are excluded for clarity.

Without sunlight exposure (Fig. 3, top left panel), burning removed oxygen rich compounds and unsaturated aliphatics (black dots) yielding a WAF enriched in aliphatic compounds (red dots). The O-poor unsaturated aliphatics (black dots, O/C < 0.2, 0.5 < H/C < 1.5) are likely volatile and may have been removed physically by the heating process whereas the O-rich compounds (black dots, O/C > 0.4) were likely consumed by the fire providing molecular oxygen for combustion.[59] Fire appeared to produce numerous new compounds, covering wide H/C and O/C ranges, which is expected as burning is associated with radical reactions,[60] which increase the molecular diversity.[61] This is consistent with FT-ICR MS results on the oil itself (no WAF extraction) before and after burning (Fig. S6†). After burning, the burned oil (Fig. S6c†) contains many unique molecules (Fig. S6d†) that were not present in the unburned oil (Fig. S6b†).

Sunlight appears to affect unburned and burned oil differently (Fig. 3, top right panel) as unburned oil WAF becomes enriched in oxygen poor formulae after sunlight exposure (blue dots, O/C < 0.4) whereas burned oil WAF becomes enriched in oxygen rich formulae after sunlight exposure (green dots, O/C > 0.4). Without burning (Fig. 3, bottom left panel), sunlight alone appears to photo-oxidize petroleum compounds of various types (unsaturated, aromatic, and condensed aromatic), rendering them water-soluble[62,63] and enriching the WAF composition in formulae with H/C < 0.5 (blue dots). The unique formulae of dark unburned (dark dots) may have been either photo-mineralized to CO_2 and volatile gases or have been ionizationally outcompeted by the photo-produced formulae (blue dots) to become undetectable in the light unburned WAF. Similar trends can be seen in the WAFs with burning and sequential photo-irradiation (Fig. 3, bottom right panel). Sunlight likely oxidizes water-soluble oil compounds (red dots) to yield a WAF enriched in now soluble aromatic compounds (green dots), which were likely present in the dark burned WAF but were not ionizable and remained undetectable. In summary, burning appears to remove unsaturated and oxygen rich compounds, while sunlight exposure yields oxygenated species, particularly of aromatic and condensed aromatic type. Molecular size

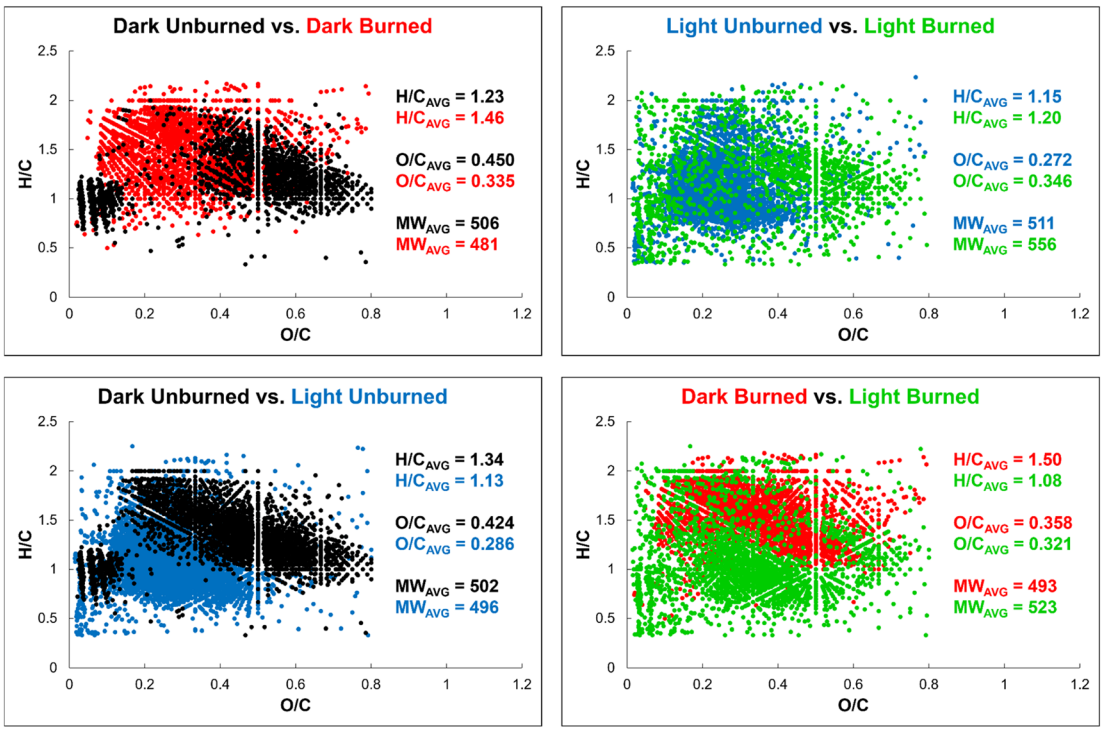

Sample	Assigned formulas	H/C_{AVG}	O/C_{AVG}	$Molecular\ Weight_{AVG}$	CHO	CHON	CHOS
Dark Unburned	3405	1.32	0.422	495	1927 (57 %)	916 (27 %)	562 (17 %)
Dark Burned	4038	1.43	0.368	484	2048 (51 %)	544 (13 %)	1446 (36 %)
Light Unburned	5022	1.15	0.308	492	2051 (41 %)	1310 (26 %)	1661 (33 %)
Light Burned	3739	1.17	0.347	501	1956 (52 %)	782 (21 %)	1001 (27 %)

Fig. 3 Van Krevelen diagrams of molecular compositions compared based on burning (top panels) and sunlight exposure (bottom panels). Plotted formulae are the only unique ones per sample among the two being compared (along with their average (AVG) H/C, O/C, and molecular weight (MW) ratios). The table below provides a summary for the bulk molecular fingerprint of each sample.

appears to not be a significant factor as the molecular fingerprinting did not reveal any major shifts in molecular weight distributions (Fig. S5†).

3.5 FT-ICR MS and optical data reveal distinct compositions between burned and unburned WAFs after sunlight exposure

To combine all data and comprehensively evaluate the chemistry occurring upon oil burning and photochemical degradation we employed principal component analysis (PCA), which explained 76% of the variance in the dataset of dark and light unburned and burned samples (Fig. 4). Five compositional classes, aliphatic, unsaturated low oxygen (ULO), unsaturated high oxygen (UHO), aromatic, and condensed aromatics (CA), derived from the FT-ICR MS data were separated based on H/C *vs.* O/C constraints to assess changes between each treatment (Table S1†).

The main driver for PCA 1 is sunlight exposure. C3, C4, and UHO classes describe the dark unburned (green) WAF fluorophoric and molecular level composition. The dark burned (blue) WAF correlates with aliphatic and C1, the light unburned (purple) WAF groups with aromatic, ULO and C2. The ULO class is typically comprised of low molecular weight acids observed after oil photo-dissolution studies and has been shown to contribute to toxicity.[54] The light burned (gold) composition comprises CA, C2, and aromatic classes. C1 and C2 are identified as oil-derived components from other studies.[53] The PCA 2 driver appears to be light and burning. The light burned WAF is negatively correlated to the unburned, signifying that burning oil produces more condensed aromatic reduced compounds after sunlight exposure than the unburned WAF.

Fig. S6† are vK plots derived from FT-ICR MS for unburned (Fig. S6a†) and burned oil (Fig. S6c†). Comparison plots were constructed to identify molecular formulae unique to each treatment in the oil. Fig. S6b† shows the unique compounds present in the unburned oil and Fig. S6d† reveal the molecular formula in the burned oil. Similar to previous findings,[10] an increase in newly formed CHON (brown dots), CHO (blue dots), and CHOS (orange dots) classes were observed in the burned oil (Fig. S6d†) compared to the unburned oil (Fig. S6b†).

Fig. 5 compares box plots for % relative abundance *versus* treatment (*i.e.* dark, light, burned or unburned samples) for carboxyl-rich alicyclic molecules (CRAM), CHO, CHON, and CHOS compositional classes in the dark unburned (green), dark burned (blue), light unburned (green), and light burned (blue). The WAF created from the unburned oil, dark unburned (green), shows higher percent relative abundances for CHO, CRAM, and CHON classes than the WAF created from the burned oil, dark burned (blue). However, the dark burned WAF had a higher abundance of CHOS species (Fig. 5). The box plots also show the presence of significantly higher percentages of CRAM in the light burned, (gold, $\rho < 0.05$) compared to the light unburned (purple), offering an explanation as to why the newly formed compounds in the oil after burning (Fig. S6d†) are not reflected in the dark and light burned WAF samples. The UHO classes for the dark WAFs had the highest percent relative abundance (% RA) compared to the light WAF samples (Fig. S4† (orange)). However, the differences among the darks observed in the optical composition for C2 (Fig. S3† purple) show the appearance of newly formed signatures in the dark burned compared to the dark unburned.

Overall, the increase in toxicity is correlated with (1) increasing DOC concentrations, (2) the appearance of petroleum degradation peaks in the EEMs, and (3) the production of aromatic, ULO, and CA in the WAF after sunlight exposure

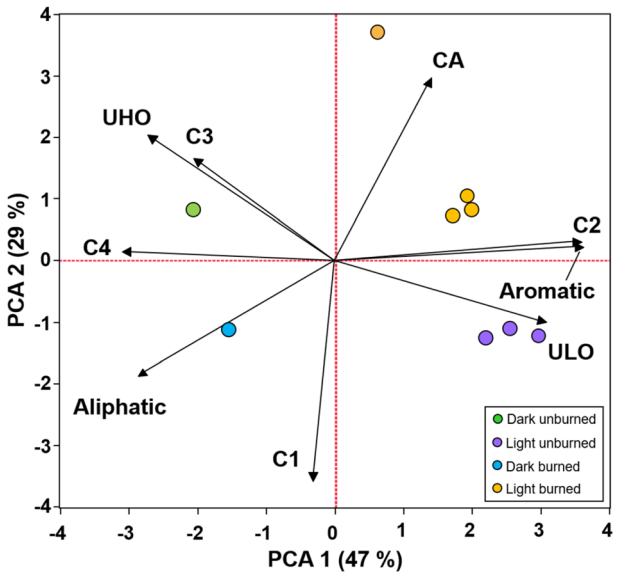

Fig. 4 PCA analysis of loadings from PARAFAC (C1–C4) and aliphatic, unsaturated low oxygen (ULO), unsaturated high oxygen (UHO), aromatic and condensed aromatic (CA) of data derived from FT-ICR MS for dark unburned (green), light unburned (purple), dark burned (blue) and light burned (gold).

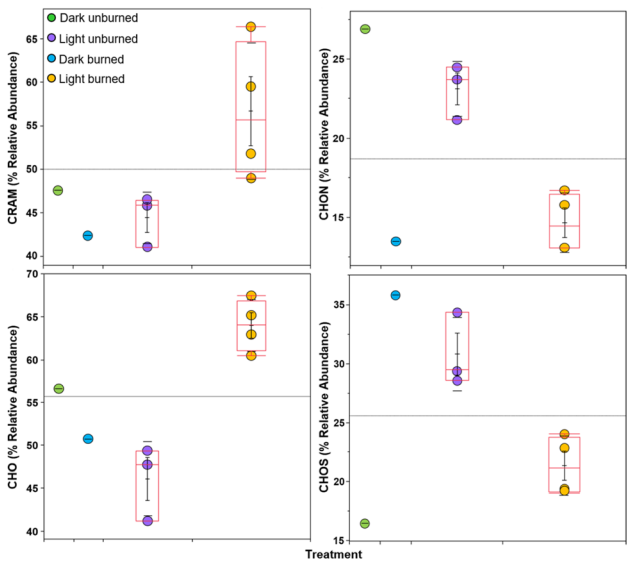

Fig. 5 Box plots of % relative abundance *versus* treatment for carboxyl-rich alicyclic molecules (CRAM), CHO, CHON, and CHOS compositional classes in the dark unburned (green), dark burned (blue), light unburned (purple), and light burned (gold) WAFs. Standard deviation (SD) was propagated for dark samples by averaging the mean SD for all replicates for each treatment.

compared to the dark for burned and unburned treatments. CRAM-like compounds have been previously identified in aqueous hydrocarbon oxidation products produced from oil.[55] The increase in CRAM-like compounds in the light burned compared to light unburned suggests that the composition of the light burned is more photorefractory, *i.e.*, reduced, which would explain the decrease in percent inhibition observed in Fig. 1 compared to the light unburned WAF. Furthermore, the DOC values and EEMs indicate that burned and unburned WAF samples differ in composition and contain oil degradation products (Fig. 2 and S3†). A decrease in CHON and CHOS classes for the light burned (gold) compared to the light unburned (purple) is observed. The decrease observed in CHOS classes in the light burned may be attributed to the fact that the burned oil residues are photorefractory and do not readily dissolve into the water after light exposure (as explained by the increase in CRAM). However, the opposite is true for the light unburned in that increases in both CHO and CHOS are observed. In line with previous findings, these data demonstrate that oxygenation occurs across a wide range of petroleum compounds after light exposure.[14] Fig. S4† illustrates the changes in individual compound classes for all treatments.

Oxygenated heteroatom classes with N and S reveal compositional changes due to burning and light exposure (Fig. 5). A decrease in % RA for the CHO classes was observed for the light unburned WAF (purple) but increased in the light burned WAF (gold) after light exposure. CHON classes also decreased for light unburned (purple) but increased for light burned (gold) when compared to their respective darks. Newly formed CHOS formulae were also observed in the burned oil (Fig. S6†), corroborating with the findings for the WAF fractions (Fig. 3). While CHOS compounds were at similar % RA in both the light unburned (purple) and dark burned WAF blue, a comparison among the molecular formulae revealed Eevidence of newly formed CHOS species (Fig. S7†). This suggests that oxygenation occurs across a wide range of compounds as shown previously.[10] The decrease in CHOS species observed in the burned WAF after light exposure (gold) suggests the burned CHOS species were photolabile and the CHO and CHON species in the burned samples are more photorefractory. More research is needed to directly correlate the increase in sulfur species and their contribution to inhibition of bacterial growth.

4 Conclusions

The toxicity of burning oil measured as a function of microbial production was not affected by dark-incubated samples. However, after light exposure, photo-enhanced toxicity was observed through inhibition of microbial production. The magnitude of photo-enhanced toxicity was reduced upon burning, which suggests the removal of some photodegradation products through burning. Increased DOC concentrations for light-exposed unburned and burned WAF, correlate to increased bacterial growth inhibition. Optical analyses revealed petroleum-derived photo and degradation fluorescence signatures. Increasing HIX values after light exposure in both WAF samples were consistent with increasing aromaticity and oxygen content confirmed by the FT-ICR-MS data. After burning, surrogate oil retained significant toxicity when water-accommodated fractions were exposed to sunlight compared to the controls. Molecular formula derived from FT-ICR- MS identified newly formed compound classes possibly contributing to residual toxicity. Overall, burning removed low MW and aliphatic compounds enriching aromatic species. The key findings from this study show that a combination of sunlight exposure and oil burning produce water-accommodated fractions that retain residual toxicity.

Author contributions

Pamela P. Benz contributed to preparation of the published work, data analysis, management and coordination responsibility for the research activity planning and execution. Phoebe Zito contributed to preparation of the published work, sample and data analysis. Ed Osborn contributed by performing experiments and data collection. Aleksandar I. Goranov contributed to preparation of the published work, sample and data analysis. Patrick G. Hatcher contributed to published work through sample and data analysis. Matthew D. Seivert contributed to planning and preparation of the initial manuscript draft. Wade H. Jeffrey contributed to preparation of the published work, sample and data analysis.

Conflicts of interest

There are no conflicts to declare.

Acknowledgements

Funding was provided by the UWF Faculty Scholarly and Creative Activity Award and a grant from BP/The Gulf of Mexico Research Initiative as part of the DEEP-C and C-IMAGE consortia. This research was also supported by NSF DMR 11-54790 State of Florida grant. A portion of this work was performed at the National High Magnetic Field Laboratory ICR User Facility, which is supported by the National Science Foundation Division of Chemistry through DMR-1644779 and the State of Florida. The authors acknowledge Dr Amy McKenna for assistance with data collection. E.O. stipend is supported by Tolmas Scholar in College of Sciences Undergraduate Research Program (CoSURP) at UNO.

References

1 Z. Tao, S. Bullard and C. Arias, High numbers of Vibrio vulnificus in tar balls collected from oiled areas of the north-central Gulf of Mexico following the 2010 BP Deepwater Horizon oil spill, *Ecohealth*, 2011, **8**, 507–511, DOI: 10.1007/s10393-011-0720-z.
2 J. L. Ramseur, *Deepwater Horizon Oil Spill: The Fate of the Oil*, Congressional Research Service, 2010.
3 J. Rullkötter and J. W. Farrington, What Was Released? Assessing the Physical Properties and Chemical Composition of Petroleum and Products of Burned Oil,

Oceanography, 2021, **34**, 44–57, DOI: 10.5670/oceanog.2021.116.

4 S. A. Stout and J. R. Payne, A critical review of marine snow in the context of oil spills and oil spill dispersant treatment with focus on the Deepwater Horizon oil spill, *Mar. Pollut. Bull.*, 2016, **108**, 186–202, DOI: 10.1016/j.marpolbul.2018.07.028.

5 E. B. Overton, T. L. Wade, J. R. Radović, B. M. Meyer, M. S. Miles and S. R. Larter, Chemical Composition of Macondo and Other Crude Oils and Compositional Alterations During Oil Spills, *Oceanography*, 2016, **29**, 50–63, DOI: 10.5670/oceanog.2016.62.

6 E. P. Blanco-Donado, I. L. Schneider, P. Artaxo, J. Lozano-Osorio, L. Portz and M. L. Oliveira, Source identification and global implications of black carbon, *Geosci. Front.*, 2022, **13**, 101149, DOI: 10.1016/j.gsf.2021.101149.

7 S. Chowdhury, A. Pozzer, A. Haines, K. Klingmueller, T. Muenzel, P. Paasonen, A. Sharma, C. Venkataraman and J. Lelieveld, *Environ. Int.*, 2022, **159**, 107020, DOI: 10.1016/j.envint.2021.107020.

8 D. T. Seymour, A. G. Verbeek, S. E. Hrudey and P. M. Fedorak, Global health burden of ambient PM2.5 and the contribution of anthropogenic black carbon and organic aerosols, *Environ. Toxicol. Chem.: Int. J.*, 1997, **16**, 658–665, DOI: 10.1002/etc.5620160409.

9 A. Luch, *The Carcinogenic Effects of Polycyclic Aromatic Hydrocarbons*, World Scientific, 2005.

10 A. Jaggi, J. R. Radović, L. R. Snowdon, S. R. Larter and T. B. Oldenburg, Composition of the dissolved organic matter produced during in situ burning of spilled oil, *Org. Geochem.*, 2019, **138**, 103926, DOI: 10.1016/j.orggeochem.2019.103926.

11 J. S. Arey, R. K. Nelson and C. M. Reddy, Disentangling Oil Weathering Using GC×GC. 2. Mass Transfer Calculations, *Environ. Sci. Technol.*, 2007, **41**, 5738–5746, DOI: 10.1021/es070006p.

12 D. C. Palacio Lozano, R. Gavard, J. P. Arenas-Diaz, M. J. Thomas, D. D. Stranz, E. Mejía-Ospino, A. Guzman, S. E. F. Spencer, D. Rossell and M. P. Barrow, Pushing the analytical limits: new insights into complex mixtures using mass spectra segments of constant ultrahigh resolving power, *Chem. Sci.*, 2019, **10**, 6966–6978, DOI: 10.1039/C9SC02903F.

13 A. K. Huba and P. R. Gardinali, Characterization of a crude oil weathering series by ultrahigh-resolution mass spectrometry using multiple ionization modes, *Sci. Total Environ.*, 2016, **563**, 600–610, DOI: 10.1016/j.scitotenv.2016.03.233.

14 P. Zito, H. Chen, D. C. Podgorski, A. M. McKenna and M. A. Tarr, Sunlight creates oxygenated species in water-soluble fractions of Deepwater horizon oil, *J. Hazard. Mater.*, 2014, **280**, 636–643, DOI: 10.1016/j.jhazmat.2014.08.059.

15 P. P. Vaughan, T. Wilson, R. Kamerman, M. E. Hagy, A. McKenna, H. Chen and W. H. Jeffrey, Photochemical changes in water accommodated fractions of MC252 and surrogate oil created during solar exposure as determined by FT-ICR MS, *Mar. Pollut. Bull.*, 2016, **104**, 262–268, DOI: 10.1016/j.marpolbul.2016.01.012.

16 M. L. Harsha, Z. C. Redman, J. Wesolowski, D. C. Podgorski and P. L. Tomco, Photochemical formation of water-soluble oxyPAHs, naphthenic acids, and other hydrocarbon oxidation products from Cook Inlet, Alaska crude oil and diesel in simulated seawater spills, *Environ. Sci.: Adv.*, 2023, **2**, 447–461, DOI: 10.1039/D2VA00325B.

17 T. Ghislain, P. Faure and R. Michels, Detection and Monitoring of PAH and Oxy-PAHs by High Resolution Mass Spectrometry: Comparison of ESI, APCI and APPI Source Detection, *J. Am. Soc. Mass Spectrom.*, 2012, **23**, 530–536, DOI: 10.1007/s13361-011-0304-8.

18 P. Zito, D. F. Smith, X. Cao, R. Ghannam and M. A. Tarr, Barium ion adduct mass spectrometry to identify carboxylic acid photoproducts from crude oil–water systems under solar irradiation, *Environ. Sci.: Processes Impacts*, 2020, **22**, 2313–2321, DOI: 10.1039/D0EM00390E.

19 M. P. Barrow, J. V. Headley, K. M. Peru and P. J. Derrick, Fourier transform ion cyclotron resonance mass spectrometry of principal components in oilsands naphthenic acids, *J. Chromatogr. A*, 2004, **1058**, 51–59, DOI: 10.1016/j.chroma.2004.08.082.

20 J. V. Headley, M. P. Barrow, K. M. Peru, B. Fahlman, R. A. Frank, G. Bickerton, M. E. McMaster, J. Parrott and L. M. Hewitt, Preliminary fingerprinting of Athabasca oil sands polar organics in environmental samples using electrospray ionization Fourier transform ion cyclotron resonance mass spectrometry, *Rapid Commun. Mass Spectrom.*, 2011, **25**, 1899–1909, DOI: 10.1002/rcm.5062.

21 J. V. Headley, K. M. Peru and M. P. Barrow, Mass spectrometric characterization of naphthenic acids in environmental samples: a review, *Mass Spectrom. Rev.*, 2009, **28**, 121–134, DOI: 10.1002/mas.20185.

22 J. V. Headley, K. M. Peru, M. P. Barrow and P. J. Derrick, Characterization of Naphthenic Acids from Athabasca Oil Sands Using Electrospray Ionization: The Significant Influence of Solvents, *Anal. Chem.*, 2007, **79**, 6222–6229. doi.org/10.1021/ac070905w.

23 J. V. Headley, K. M. Peru, B. Fahlman, A. Colodey and D. W. McMartin, Selective solvent extraction and characterization of the acid extractable fraction of Athabasca oils sands process waters by Orbitrap mass spectrometry, *Int. J. Mass Spectrom.*, 2013, **345–347**, 104–108, DOI: 10.1016/j.ijms.2012.08.023.

24 X. Cao and M. A. Tarr, Aldehyde and Ketone Photoproducts from Solar-Irradiated Crude Oil–Seawater Systems Determined by Electrospray Ionization–Tandem Mass Spectrometry, *Environ. Sci. Technol.*, 2017, **51**, 11858–11866, DOI: 10.1021/acs.est.7b01991.

25 S. F. Niles, M. L. Chacón-Patiño, H. Chen, A. M. McKenna, G. T. Blakney, R. P. Rodgers and A. G. Marshall, Molecular-Level Characterization of Oil-Soluble Ketone/Aldehyde Photo-Oxidation Products by Fourier Transform Ion Cyclotron Resonance Mass Spectrometry Reveals Similarity Between Microcosm and Field Samples, *Environ. Sci. Technol.*, 2019, **53**, 6887–6894, DOI: 10.1021/acs.est.9b00908.

26 L. Faksness, D. Altin, T. Nordug, P. Daling and B. H. Hansen, Chemical comparison and acute toxicity of water accommodated fraction (WAF) of source and field collected Macondo oils from the Deepwater Horizon spill, *Mar. Pollut. Bull.*, 2015, **91**, 222–229, DOI: 10.1016/j.marpolbul.2014.12.002.

27 T. Parkerton, M. Boufadel, T. Nordtug, C. Mitchelmore, K. Colvin, D. Wetzel, M. G. Barron, G. E. Bragin, B. de Jourdan and J. Loughery, Recommendations for advancing media preparation methods used to assess aquatic hazards of oils and spill response agents, *Aquat. Toxicol.*, 2023, **259**, 106518, DOI: 10.1016/j.aquatox.2023.106518.

28 D. C. Smith and F. Azam, A simple, economical method for measuring bacterial protein synthesis rates in seawater using 3H-leucine, *Mar. Microb. Food Webs*, 1992, **6**, 107–114.

29 P. Matrai, M. Vernet, R. Hood, A. Jennings, E. Brody and S. Saemundsdottir, Light-dependence of carbon and sulfur production by polar clones of the genus Phaeocystis, *Mar. Biol.*, 1995, **124**, 157–167, DOI: 10.1007/BF00349157.

30 R. G. M. Spencer, L. Bolton and A. Baker, Freeze/thaw and pH effects on freshwater dissolved organic matter fluorescence and absorbance properties from a number of UK locations, *Water Res.*, 2007, **41**, 2941–2950, DOI: 10.1016/j.watres.2007.04.012.

31 P. Zito, D. C. Podgorski, J. Johnson, H. Chen, R. P. Rodgers, F. Guillemette, A. M. Kellerman, R. G. M. Spencer and M. A. Tan, Molecular-Level Composition and Acute Toxicity of Photosolubilized Petrogenic Carbon, *Environ. Sci. Technol.*, 2019, **53**, 8235–8243, DOI: 10.1021/acs.est.9b01894.

32 K. R. Murphy, C. A. Stedmon, D. Graeber and R. Bro, Fluorescence spectroscopy and multi-way techniques. PARAFAC, *Anal. Methods*, 2013, **5**, 6557, DOI: 10.1039/C3AY41160E.

33 C. A. Stedmon and R. Bro, Characterizing dissolved organic matter fluorescence with parallel factor analysis: a tutorial, *Limnol. Oceanogr.: Methods*, 2008, **6**, 572–579, DOI: 10.4319/lom.2008.6.572.

34 K. R. Murphy, C. A. Stedmon, P. Wenig and R. Bro, OpenFluor– an online spectral library of auto-fluorescence by organic compounds in the environment, *Anal. Methods*, 2014, **6**, 658–661, DOI: 10.1039/C3AY41935E.

35 T. Ohno, J. Chorover, A. Omoike and J. Hunt, Molecular weight and humification index as predictors of adsorption for plant- and manure-derived dissolved organic matter to goethite, *Eur. J. Soil Sci.*, 2007, **58**, 125–132, DOI: 10.1111/j.1365-2389.2006.00817.x.

36 T. Dittmar, B. Koch, N. Hertkorn and G. Kattner, A simple and efficient method for the solid-phase extraction of dissolved organic matter (SPE-DOM) from seawater, *Limnol. Oceanogr.: Methods*, 2008, **6**(6), 230–235, DOI: 10.4319/lom.2008.6.230.

37 A. Goranov, A. Tadini, L. Martin-Neto, A. C. Bernardi, P. Oliveira, J. Pezzopane, D. Milori, S. Mounier and P. G. Hatcher, Comparison of Sample Preparation Techniques for the (−)ESI-FT-ICR-MS Analysis of Humic and Fulvic Acids, *Environ. Sci. Technol.*, 2022, **56**(17), 12688–12701, DOI: 10.1021/acs.est.2c01125.

38 J. A. Hawkes, J. D'Andrilli, J. N. Agar, M. P. Barrow, S. M. Berg, N. Catalán, H. Chen, R. K. Chu, R. B. Cole, T. Dittmar, R. Gavard, G. Gleixner, P. G. Hatcher, C. He, N. J. Hess, R. H. S. Hutchins, A. Ijaz, H. E. Jones, W. Kew, M. Khaksari, D. C. Palacio Lozano, J. Lv, L. R. Mazzoleni, B. E. Noriega-Ortega, H. Osterholz, N. Radoman, C. K. Remucal, N. D. Schmitt, S. K. Schum, Q. Shi, C. Simon, G. Singer, R. L. Sleighter, A. Stubbins, M. J. Thomas, N. Tolic, S. Zhang, P. Zito and D. C. Podgorski, An international laboratory comparison of dissolved organic matter composition by high resolution mass spectrometry: are we getting the same answer?, *Limnol. Oceanogr.: Methods*, 2020, **18**, 235–258, DOI: 10.1002/lom3.10364.

39 R. L. Sleighter and P. G. Hatcher, Molecular characterization of dissolved organic matter (DOM) along a river to ocean transect of the lower Chesapeake Bay by ultrahigh resolution electrospray ionization Fourier transform ion cyclotron resonance mass spectrometry, *Mar. Chem.*, 2008, **110**, 140–152, DOI: 10.1016/j.marchem.2008.04.008.

40 A. I. Goranov, R. L. Sleighter, D. A. Yordanov and P. G. Hatcher, TEnvR: MATLAB-based toolbox for environmental research, *Anal. Methods*, 2023, **15**, 5390–5400, DOI: 10.1039/D3AY00750B.

41 J. Merder, J. A. Freund, U. Feudel, J. Niggemann, G. Singer and T. Dittmar, Improved Mass Accuracy and Isotope Confirmation through Alignment of Ultrahigh-Resolution Mass Spectra of Complex Natural Mixtures, *Anal. Chem.*, 2019, **92**, 2558–2565, DOI: 10.1021/acs.analchem.9b04234.

42 W. A. Obeid, Investigation of the potential for algaenan to produce hydrocarbon based fuels from algae by hydrous pyrolysis, PhD thesis, Old Dominion University, 2015.

43 B. P. Koch, T. Dittmar, M. Witt and G. Kattner, Fundamentals of Molecular Formula Assignment to Ultrahigh Resolution Mass Data of Natural Organic Matter, *Anal. Chem.*, 2007, **79**, 1758–1763, DOI: 10.1021/ac061949s.

44 A. Stubbins, R. G. M. Spencer, H. Chen, P. G. Hatcher, K. Mopper, P. J. Hernes, V. L. Mwamba, A. M. Mangangu, J. N. Wabakanghanzi and J. Six, Illuminated darkness: molecular signatures of Congo River dissolved organic matter and its photochemical alteration as revealed by ultrahigh precision mass spectrometry, *Limnol. Oceanogr.*, 2010, **55**, 1467–1477, DOI: 10.4319/lo.2010.55.4.1467.

45 E. B. Kujawinski and M. D. Behn, Automated Analysis of Electrospray Ionization Fourier Transform Ion Cyclotron Resonance Mass Spectra of Natural Organic Matter, *Anal. Chem.*, 2006, **78**, 4363–4373. doi.org/10.1021/ac0600306.

46 H. Maki, T. Sasaki and S. Harayama, Photo-oxidation of biodegraded crude oil and toxicity of the photo-oxidized products, *Chemosphere*, 2001, **44**, 1145–1151, DOI: 10.1016/S0045-6535(00)00292-7.

47 J. Alan Roebuck, D. C. Podgorksi, S. Wagner and R. Jaffé, Photodissolution of charcoal and fire-impacted soil as a potential source of dissolved black carbon in aquatic environments, *Org. Geochem.*, 2017, **112**, 16–21, DOI: 10.1016/j.orggeochem.2017.06.018.

48 A. T. Roman-Hubers, C. Aeppli, J. N. Dodds, E. S. Baker, K. M. McFarlin, D. J. Letinski, L. Zhao, D. A. Mitchell, T. F. Parkerton, R. C. Prince, T. Nedwed and I. Rusyn, Temporal chemical composition changes in water below a crude oil slick irradiated with natural sunlight, *Mar. Pollut. Bull.*, 2022, **185**(pt B), 114360, DOI: **10.1016/j.marpolbul.2022.114360**.

49 B. H. Harriman, P. Zito, D. C. Podgorski, M. A. Tarr and J. M. Suflita, Impact of Photooxidation and Biodegradation on the Fate of Oil Spilled During the Deepwater Horizon Incident: Advanced Stages of Weathering, *Environ. Sci. Technol.*, 2017, **51**, 7412–7421. **doi.org/10.1021/acs.est.7b01278**.

50 P. Zito, D. C. Podgorski and M. A. Tarr, Emerging Chemical Methods for Petroleum and Petroleum-Derived Dissolved Organic Matter Following the Deepwater Horizon Oil Spill, *Annu. Rev. Anal. Chem.*, 2023, **16**, 429–450, DOI: **10.1146/annurev-anchem-091522-110825**.

51 A. Zsolnay, E. Baigar, M. Jimenez, B. Steinweg and F. Saccomandi, Differentiating with fluorescence spectroscopy the sources of dissolved organic matter in soils subjected to drying, *Chemosphere*, 1999, **38**, 45–50, DOI: **10.1016/S0045-6535(98)00166-0**.

52 J. R. Helms, D. A. Glinski, R. N. Mead, M. W. Southwell, G. B. Avery, R. J. Kieber and S. A. Skrabal, Photochemical dissolution of organic matter from resuspended sediments: impact of source and diagenetic state on photorelease, *Org. Geochem.*, 2014, **73**, 83–89, DOI: **10.1016/j.orggeochem.2014.05.011**.

53 Z. Zhou, L. Guo and C. L. Osburn, in *Hydrocarbon and Lipid Microbiology Protocols: Petroleum, Hydrocarbon and Lipid Analysis*, ed. T. J. McGenity, K. N. Timmis and B. Nogales, Springer Berlin Heidelberg, Berlin, Heidelberg, 2017, pp. 179–200, DOI: **10.1007/8623_2015_137**.

54 D. C. Podgorski, P. Zito, J. T. McGuire, D. Martinovic-Weigelt, I. M. Cozzarelli, B. A. Bekins and R. G. M. Spencer, Examining Natural Attenuation and Acute Toxicity of Petroleum-Derived Dissolved Organic Matter with Optical Spectroscopy, *Environ. Sci. Technol.*, 2018, **52**, 6157–6166, DOI: **10.1021/acs.est.8b0001**.

55 D. C. Podgorski, J. Walley, M. P. Shields, D. Hebert, M. L. Harsha, R. G. M. Spencer, M. A. Tarr and P. Zito, Dispersant-enhanced photodissolution of Macondo crude oil: a molecular perspective, *J. Hazard. Mater.*, 2024, **461**, 132558, DOI: **10.1016/j.jhazmat.2023.13255**.

56 E. A. Whisenhant, P. Zito, D. C. Podgorski, A. M. McKenna, Z. C. Redman and P. L. Tomco, Unique Molecular Features of Water-Soluble Photo-Oxidation Products among Refined Fuels, Crude Oil, and Herded Burnt Residue under High Latitude Conditions, *ACS ES&T Water*, 2022, **2**(6), 994–1002, DOI: **10.1021/acsestwater.1c00494**.

57 R. L. Sleighter, H. Chen, A. S. Wozniak, A. S. Willoughby, P. Caricasole and P. G. Hatcher, Establishing a Measure of Reproducibility of Ultrahigh-Resolution Mass Spectra for Complex Mixtures of Natural Organic Matter, *Anal. Chem.*, 2012, **84**(21), 9184–9191, DOI: **10.1021/ac3018026**.

58 S. Kim, R. W. Kramer and P. G. Hatcher, Graphical Method for Analysis of Ultrahigh-Resolution Broadband Mass Spectra of Natural Organic Matter, the Van Krevelen Diagram, *Anal. Chem.*, 2003, **75**(20), 5336–5344, DOI: **10.1021/ac034415p**.

59 K. W. Bostick, A. R. Zimmerman, A. S. Wozniak, S. Mitra and P. G. Hatcher, Production and composition of pyrogenic dissolved organic matter from a logical series of laboratory-generated chars, *Front. Earth Sci.*, 2018, **6**(43), 1–14, DOI: **10.3389/feart.2018.00043**.

60 H. Richter and J. B. Howard, Formation of polycyclic aromatic hydrocarbons and their growth to soot – a review of chemical reaction pathways, *Prog. Energy Combust. Sci.*, 2000, **26**(4–6), 565–608, DOI: **10.1016/S0360-1285(00)00009-5**.

61 A. I. Goranov, A. S. Wozniak, K. W. Bostick, A. R. Zimmerman, S. Mitra and P. G. Hatcher, Microbial labilization and diversification of pyrogenic dissolved organic matter, *Biogeosciences*, 2022, **19**(5), 1491–1514, DOI: **10.5194/bg-19-1491-2022**.

62 A. I. Goranov, A. S. Wozniak, K. W. Bostick, A. R. Zimmerman, S. Mitra and P. G. Hatcher, Photochemistry after fire: structural transformations of pyrogenic dissolved organic matter elucidated by advanced analytical techniques, *Geochim. Cosmochim. Acta*, 2020, **290**, 271–292, DOI: **10.1016/j.gca.2020.08.030**.

63 J. A. Roebuck, D. C. Podgorksi, S. Wagner and R. Jaffe, Photodissolution of charcoal and fire-impacted soil as a potential source of dissolved black carbon in aquatic environments, *Org. Geochem.*, 2017, **112**, 16–21, DOI: **10.1016/j.orggeochem.2017.06.018**.